Proceedings of 3rd International Conference on Violent Flows (VF-2016)
9-11, March 2016, Osaka, Japan

An experimental investigation on the influence of the temporal variation of freak wave geometry on the elastic response of a container ship

Hidetaka Houtani[1], Katsuji Tanizawa[1], Takuji Waseda[2] and Hiroshi Sawada[1]
[1]*National Maritime Research Institute, Tokyo, Japan*
[2]*The University of Tokyo, Chiba, Japan*

Abstract

Recent studies have revealed that in addition to the height of a freak wave the asymmetry of the spatial profile of a freak wave evolves in time. Therefore, it is deduced that the structural response of a ship is strongly affected by the timing of the encounter of a ship with a freak wave. To verify this deduction, we conducted a towing tank experiment using an elastic model of a container ship.

Unidirectional modulational wave trains and freak waves in unidirectional irregular waves were produced in the Actual Sea Model Basin of the National Maritime Research Institute. We developed a wave generation method based on the higher-order spectral method (HOSM-WG) because the nonlinear process of quasi-resonant interaction plays an important role in the generation of freak waves. An elastic model ship whose L_{pp} is 4.0 m was used in the experiment. The longitudinal distribution of the vertical bending stiffness and the height of the neutral axis were designed to be similar to the subject container ship. The similarity was validated by the three-point bending test and the hammering test.

Whipping responses due to slamming were measured. The peak wavelength of the wave trains was 4.0 m (peak wave period is 1.6 sec). The timing of the encounter was shifted over 2 sec at 0.2 sec interval. During the shift, the geometry of a freak wave varies from leaning forward to leaning backward, and the largest variation of the encounter wave height was over 8 cm (14.6 - 22.9 cm) in an irregular wave case. This experiment showed that the timing of the encounter significantly affects the maximum sagging moment and that the value of the maximum sagging moment strongly depends on the zero-up-cross encounter wave height of a freak wave.

Keywords: Freak wave; Wave geometry; Slamming; Whipping; Elastic model; Vertical bending moment; HOSM-WG

1 Introduction

Recent studies have shown that the probability of freak wave occurrence increases due to the prominence of quasi-resonant interaction (nonlinear wave-wave interaction) as the directional spreading and the frequency bandwidth of a spectrum narrow (e.g. Janssen [1], Mori and Janssen. [2], Waseda *et al*. [3]). A wave group in an irregular wave field evolves due to quasi-resonant interaction, and accordingly a freak wave appears. Generation and evolution of wave groups have been studied in detail regarding the modulational instability of a Stokes' wave (e.g. Benjamin *et al*. [4]).

Freak waves potentially have a devastating effect on the longitudinal strength of a ship. The encounter of a ship with a freak wave can cause a significant vertical bending moment. Yamamoto *et al.* [5] analyzed an accident of a bulk carrier near Japan in 1980. They reported that the significant vertical bending moment could be caused by slamming when the ship encountered a large wave. They indicated that this significant bending moment could split the bulk carrier. Clauss *et al*. [6] indicated that the local geometry of a freak wave including wavelength, crest front steepness, crest-trough asymmetry and, of course, wave height, affects the vertical bending moment on a ship.

Analysis of the accident of a bulk carrier by Yamamoto *et al*. [5] assumed that the large wave that encountered the bulk carrier propagated without changing its geometry. However, the geometry of a wave actually varies due to its dispersive property. Fedele [7] investigated the geometry variation of a wave in a Gaussian envelope wave group. He reported that the wave initially leans forward and becomes symmetric when the crest height is maximum. It then leans backward. A similar tendency in wave geometry variation was observed in dispersive focusing waves (Kurimoto [8], Banner *et al*. [9]) with modulational wave trains (Houtani *et al*. [10]).

Fig. 1 shows the spatiotemporal variation of the geometry of a modulational wave trains (BF7; parameters of this wave train will be mentioned in §2.3.1). The t_{max} and x_{max} denote when and where the crest height is maximum. In the vicinity of the crest height maximum, a

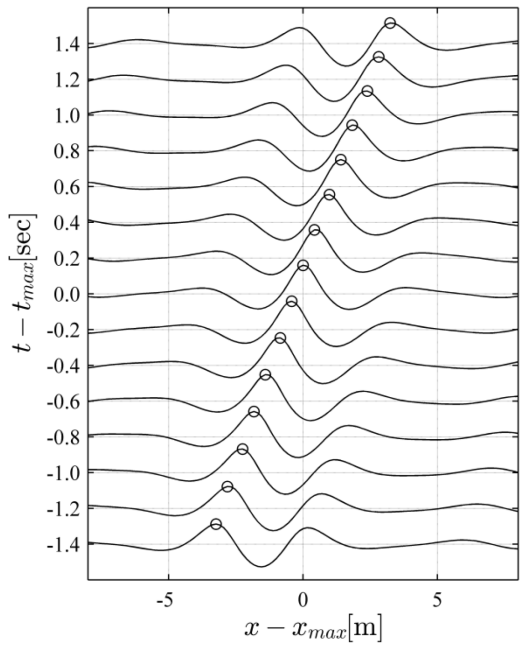

Fig. 1 Temporal evolution of the geometry of a modulational wave train. ○: crest position.

large variation of the wave geometry from leaning forward ($t < t_{max}$) to leaning backward ($t > t_{max}$) over a two wave period (3.2 sec) is seen. During this geometry variation, a sharrow trough in front of the crest and a deep trough behind the crest are observed when $t < t_{max}$, and vice versa when $t > t_{max}$. In a head sea, slamming occurs when a ship reenters the water after it hits the crest of a freak wave. Therefore, it is deduced that it is most dangerous for a ship to encounter a freak wave slightly after the time of the crest height maximum when the trough behind the crest is deepest.

Here, we experimentally investigated the influence of the temporal variation of freak wave geometry on the elastic response of a container ship. In this experiment, the timing of the encounter of an elastic model ship with a freak wave was shifted, and the vertical bending moments were measured.

A towing tank experiment using an elastic model was conducted to clarify the influence of the temporal variation of freak wave geometry on the elastic response of a container ship. Here, the effect of the timing of the encounter of a container ship with a freak wave on the maximum sagging moments is reported.

2 Experiments

2.1 Facility

The towing experiment was carried out in the Actual Sea Model Basin (ASMB) at the National Maritime Research Institute (see Tanizawa *et al*. [11]). The basin is 80.0m in length, 40.0m in width and 4.5m in depth. It is fully surrounded by 382 flaps with wave-absorbing capacity. This experimental facility can synchronously control the wave makers and the towing carriage by computer.

Table 1 Principal dimensions of the subject ship and the model

	Ship	Model
Length L_{pp} [m]	283.8	4.000
Breadth B [m]	42.80	0.6032
Depth d [m]	14.00	0.1973
Draft D [m]	24.00	0.3383

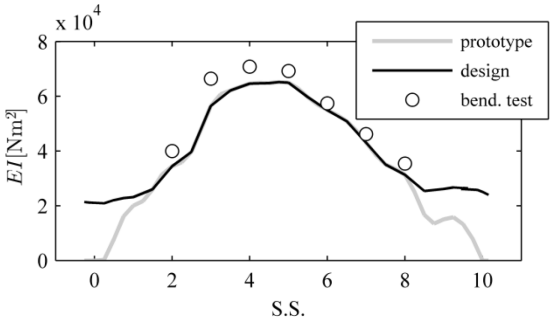

Fig. 2 The longitudinal distribution of the vertical bending stiffness of the model ship.

Table 2 Natural frequency of the model ship (unit: Hz).

	calculation		model ship (ham. test)
	(i)	(ii)	
2-node	4.673	5.302	5.273
3-node	12.08	12.20	10.55
4-node	-	21.92	-

Therefore, the timing of the encounter of a model ship with a freak wave can be systematically and accurately shifted.

2.2 Model experiment

The principal dimensions of the subject container ship (6,600 TEU) are shown in Table 1. The scale of the model is 1/70.95.

An elastic model that satisfies the similarity of the elastic response was made to measure the vertical bending moment including elastic vibration on a ship. The hull was made of urethane foam, and the metal beam is equipped such that the longitudinal distribution of the vertical bending stiffness and the height of the neutral axis were similar to the subject ship. The design details of the elastic model ship are shown in the Appendix.

A three-point bending test was conducted to evaluate the vertical bending stiffness (EI) of the model ship. The longitudinal distribution of EI of the model ship is compared with those of the prototype and the design in Fig. 2. The similarity in the vertical bending stiffness is valid.

A hammering test was conducted to evaluate the natural frequency of the vertical vibration mode of the model ship. The natural frequency of the model ship is compared with the following calculations as in Table 2:

(i) A theoretical calculation that considers the longitudinal distribution of the weights and the vertical bending stiffness. The natural vibration mode is assumed to be of the uniform beam (Yamamoto *et al*. [12]).

(ii) Calculation by NASTRAN (lumped-mass system).

The natural frequency—especially the two-node natural frequency—of the model ship agrees well with that of the

calculations in Table 2. The three-point bending test and the hammering test results show that the model ship mimics the elastic characteristics of the subject ship.

In the towing experiment, only the heave and the pitch motion were allowed. We measured vertical bending moment at each square station (from S.S.2 to S.S.8) as well as heave, pitch, vertical acceleration at F.P. and encounter wave elevation at S.S.5. The encounter wave was measured sufficiently apart from the model ship where there was almost no influence of the wave generated by the model ship. The model ship was towed at 0.727 m/s (Fn = 0.116) corresponding to 12 knots.

In each test, the ship was towed so that the mid-ship (and F.P. in one case) met the maximum crest position at each time (denoted as ○ in Fig. 1). The timing of the encounter was shifted over 2 sec at 0.2 sec intervals.

2.3 Generated waves

Unidirectional modulational wave trains and freak waves in unidirectional irregular waves were produced in the ASMB. The wave generation method will be explained in §2.4.

The definition of the wave height in this paper is shown in Fig. 3. The wave whose crest height is maximum is defined as #2. Wave #1 is defined as a wave just in front of the wave #2. The front wave height H_f and the rear wave height H_r are defined in front of and behind the crest (that correspond to the zero-up-crossing and the zero-down-crossing wave heights in space); C is crest height. The subscript numbers 1 and 2 denote waves #1 and #2 respectively.

The temporal variation of the geometry of the modulational wave trains and the irregular waves are mentioned below.

2.3.1 Modulational wave trains

The initial profile $\zeta(x)$ of the modulational wave trains were given as

$$\zeta(x) = a_c \cos(k_c x) + b_+ \cos(k_+ x + \varphi_+) + b_- \cos(k_- x + \varphi_-). \quad (1)$$

Here, subscripts c, +, and - denote the carrier wave component, upper sideband component and lower sideband component, respectively. Terms a and b are amplitude, k is wavenumber, and $k_\pm = k_c \pm \Delta k$ where Δk is perturbation wavenumber. Initial values were set as follows: carrier wavelength $2\pi/k_c = 4.0$ (m), wave steepness $a_0 k_c = 0.08$ with $a_0 = (a_c^2 + b_+^2 + b_-^2)^{1/2}$ and phase $\varphi_\pm = -\pi/4$. In this study, perturbation wavenumber $k_c/\Delta k$ was set to 7 and 9, and denotes these cases as BF7 and BF9 hereafter. $k_c/\Delta k$ represents the number of waves in a wave group.

The temporal evolution of the wave height H_{2f} and H_{2r} and the crest height C_2 of BF7 and BF9 are shown in Fig. 4. The t = 60 sec (= t_{max}) is the time of the crest height maximum. In both cases, the front wave height H_f is higher than the rear wave height H_r when $t < t_{max}$. On the other hand, H_r is higher than H_f when $t > t_{max}$.

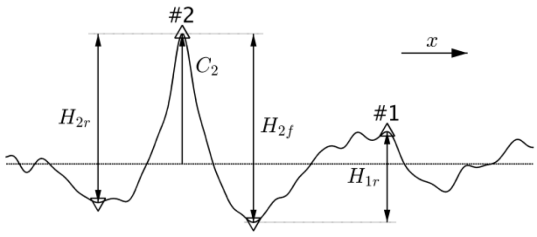

Fig. 3 Definitions of wave heights

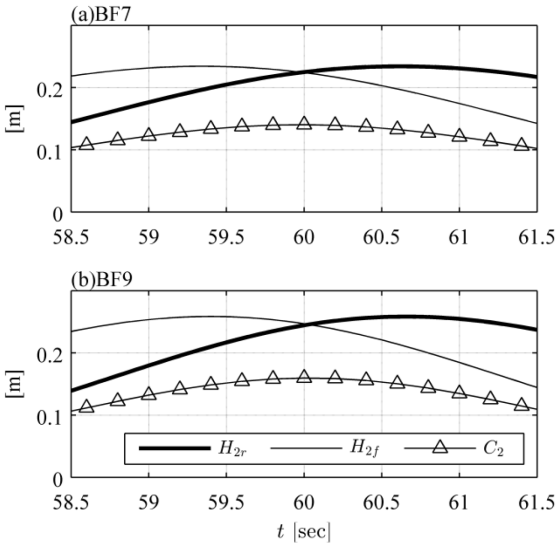

Fig. 4 Temporal evolution of the wave heights (H_{2r} and H_{2f}) and crest height (C_2). (a) case BF7, (b) case BF9.

2.3.2 Freak waves in unidirectional irregular waves

The initial profile $\zeta(x)$ of the unidirectional irregular waves were given with the JONSWAP spectrum:

$$S(f) = \frac{\alpha g^2}{(2\pi)^4 f^5} \exp\left\{-1.25\left(\frac{f_p}{f}\right)^4\right\} \gamma^{\exp\left\{\frac{(f/f_p-1)^2}{2\sigma^2}\right\}} \quad (2)$$
$$\left(\sigma = \begin{cases} 0.07 & (\text{for } f < f_p) \\ 0.09 & (\text{for } f < f_p) \end{cases}\right).$$

Peak frequency f_p was set so that the peak wavelength $2\pi/k_p$ was 4.0 m. Parameter γ that is related to the frequency bandwidth was set to 3 and 20, and denoted these cases as irr3 and irr20 hereafter. Parameter α was set so that the wave steepness $H_s k_p/2$ was 0.10 where H_s denotes the significant wave height.

The temporal evolution of the wave height H_{2f} and H_{2r} and the crest height C_2 of irr3 and irr20 are shown in Fig. 5. t = 60 sec (= t_{max}) is the time of the crest height maximum. Here, H_{2f}, H_{2r} and C_2 are obtained by zero-crossing analysis. The maximum crest or trough within the successive zero-crossing points can change during the wave evolution. Therefore, jumps in the values appear in Fig. 5. As with the case of the modulational wave trains, the front wave height H_f is higher than the rear wave height H_r roughly

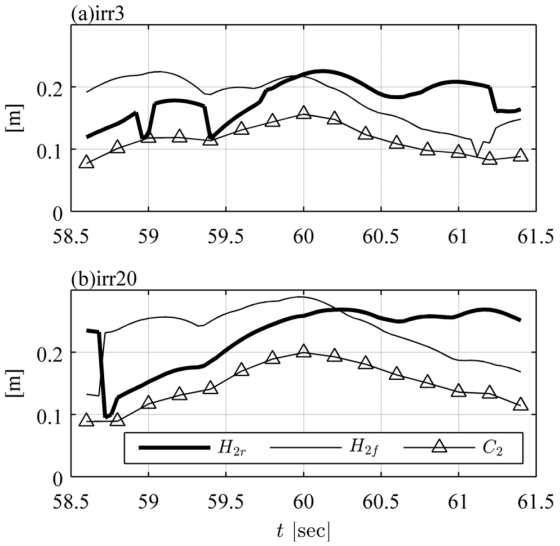

Fig. 5 Temporal evolution of the wave heights (H_{2r} and H_{2f}) and crest height (C_2). (a) case irr3, (b) case irr20.

when $t < t_{max}$. On the other hand, H_r is higher than H_f roughly when $t > t_{max}$ both in irr3 and irr20.

2.4 Wave generation method (HOSM-WG)

The waves described in §2.3.1 and §2.3.2 were generated in the ASMB by the HOSM-WG method (Waseda *et al*. [13], Houtani *et al*. [14]). HOSM-WG reproduces the nonlinear temporal evolution of the wave field simulated by the higher-order spectral method (HOSM; West *et al*. [15], Dommermuth *et al*. [16]) in an experimental wave basin.

The wave maker signal is calculated with the Biesel's transfer function (Biesel *et al*. [17]) applied to the output of an HOSM simulation. Biesel's transfer function is the analytical transfer function between the flap motion and the amplitude of the generated waves. This wave maker signal evolves in time in accordance with the wave fields simulated by HOSM. The generated wave fields are periodic in space reflecting the spatial periodic boundary condition of the HOSM simulation.

In the HOSM-WG, the wave fields are sufficiently evolved due to the quasi-resonant interaction simulated by the HOSM. This can be used in the calculation of the wave maker signals. Therefore, sufficiently evolved wave fields can be produced in a wave basin whose spatial scale is of $O(\varepsilon^{-1}k_p^{-1})$ where ε denotes the representative wave steepness. It is also advantageous that we can control when and where the target wave (e.g. freak wave) appears in the basin. In this study, waves were generated so that the crest reached its maximum at $t = 60$ sec.

3 Results and Discussion

Here, the results of the towing experiment with the elastic model ship are shown, and the influence of the encounter timing of the model ship with a freak wave on the maximum sagging vertical bending moment will be discussed. The range of the encounter wave heights H_{1r} and H_{2r} in the experiment is shown in Table 3. (FP) in Table 3 shows the case in which the F.P. of the model ship met the maximum crest position. In other cases, the mid-ship of the model ship met the maximum crest position.

Table 3 The range of the encounter wave heights H_{1r} and H_{2r} measured in the experiment.

wave	H_{1r} [cm]	H_{2r} [cm]
BF7	8.13 - 24.46	17.19 - 24.02
BF9	7.50 - 25.88	18.90 - 26.25
irr3	2.18 - 22.46	14.57 - 22.92
irr20	9.27 - 26.47	17.49 - 28.05
BF9(FP)	5.83 - 20.12	18.49 - 26.72

3.1 Measurement of whipping

The measured time series of the vertical responses, encounter wave, heave, pitch, vertical acceleration and vertical bending moments at S.S.8, S.S.5 and S.S.2, of the model ship in the case BF7 are shown in Fig. 6. The positive values of each datum are defined as follows: vertically upward in encounter wave and heave, bow-up in pitch, vertically downward in vertical acceleration, and sagging in vertical bending moment.

The figures of the vertical bending moment in Fig. 6 clearly show that the whipping components are superimposed on the encounter wave components. The maximum sagging moments that appear when the model hits the water surface just behind the crest of the wave #1 and #2 are denoted as ● and □ in Fig. 6. These maximum sagging moments are much higher than the maximum hogging moment (see Kinoshita *et al*. [18], Minami *et al*. [19], Shi *et al*. [20]).

3.2 Maximum sagging moments

The influence of the timing of the encounter of the model ship with a freak wave on the maximum sagging moment is investigated here. The maximum sagging moments and encounter wave heights are plotted against the encounter time in Fig. 7. Here, t_e denotes the encounter timing of the model with wave #2. The maximum sagging moments caused by wave #1 (●) is also plotted against t_e though the model encounters wave #1 at one encounter wave period before t_e. In the time series, the rear wave height H_r is defined as the zero-up-crossing wave height as indicated in the top figure of Fig. 6. The ● and □ denote the encounter wave height H_{1r} and H_{2r} (left column), and also denote the maximum sagging moment that occurs just behind the crest of the wave #1 and #2 (right column).

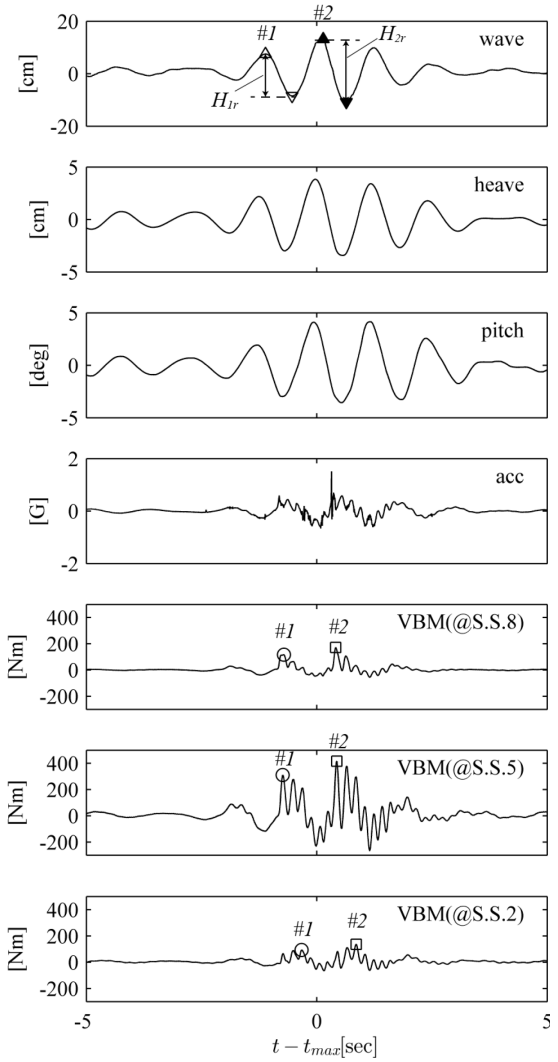

Fig. 6 Time series of the vertical responses. The model ship encountered the freak wave crest (BF7) at $t = t_{max}$.

Maximum encounter wave height H_{2r} is observed at $t_e > t_{max}$. These results can be deduced from the temporal evolution of the wave height H_{2r} that is defined in space (see Fig. 4, Fig. 5). Furthermore, it seems that the variation of the maximum sagging moment against the encounter time is similar to the variation of the encounter wave height. For example, both the maximum encounter wave height and the maximum sagging moment occurs at $t_e > t_{max}$ with regard to wave #2.

The encounter wave heights shown in Fig. 7 were measured at S.S.5. Here, the correlation between the location of the wave height measurement and the maximum sagging moment is discussed. The encounter wave heights and maximum sagging moments in BF9(FP) are shown in Fig. 8. Fig. 8(a) compares the encounter wave heights measured at S.S.5 and F.P. Clearly, the encounter wave height varies as the measurement location varies. Comparing (a) and (b) in Fig. 8, it seems that the maximum sagging moment is more correlated with the encounter wave height measured at S.S.5 than that measured at F.P. Therefore, the encountered wave height

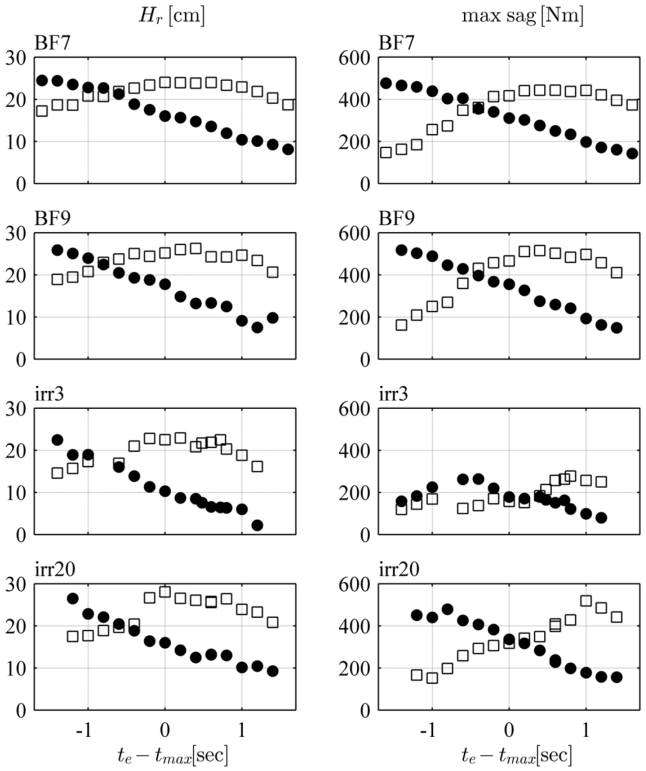

Fig. 7 Encounter wave heights (left column) and maximum sagging moments (right column) plotted against the timing of the encounter of the model ship with a freak wave. ●: wave #1, □: wave #2.

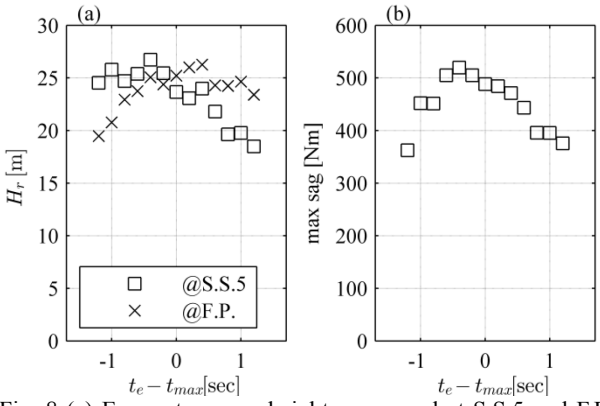

Fig. 8 (a) Encounter wave heights measured at S.S.5 and F.P. and (b) maximum sagging moments plotted against the timing of the encounter of the model ship with a freak wave (BF9(FP)). Only the results of wave #2 are shown.

measured at S.S.5 is adopted for subsequent measurements.

The maximum sagging moments measured at each square station are plotted against the encounter wave height H_r in Fig. 9 to clarify the correlation between them. The maximum sagging moment linearly increases with the encountered wave height with regard to wave #1. This linear trend partially applies to wave #2, but the much lower maximum sagging moments than this linear trend are also observed. This sort of linear trend between wave height and maximum sagging moment on a ship was reported by Kinoshita *et al*. [18] and Shi *et al*. [20].

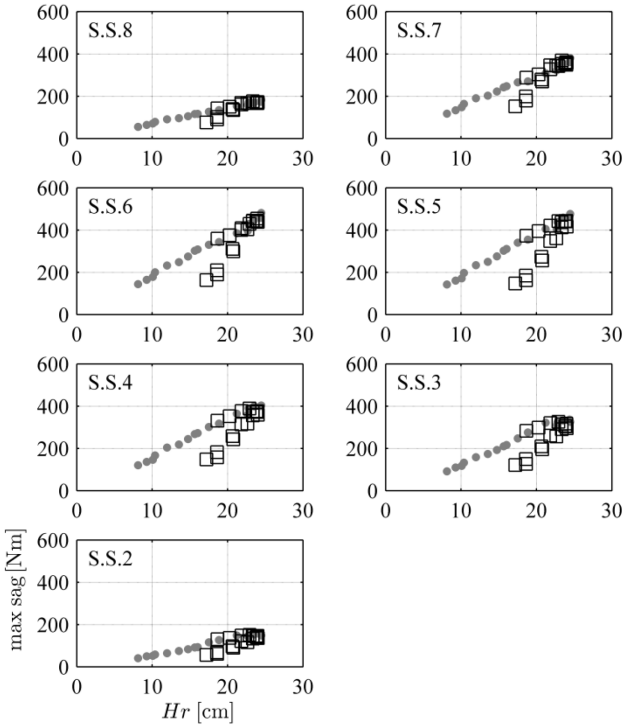

Fig. 9 Maximum sagging moments at each square station plotted against encounter wave height (BF7). ●: wave #1, □: wave #2.

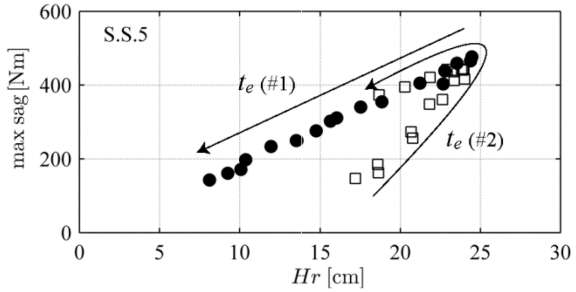

Fig. 10 Enlarged view of the S.S.5 in Fig. 9.

Fig. 10 is an enlarged view of the case S.S.5 in Fig. 9. The arrows indicate the encounter timing t_e. This figure reveals that the maximum sagging moment becomes much lower than the linear trend in the case of the early encounter timing. At early encounter timing, the maximum sagging moment that occurrs just behind crest #1 is relatively large as shown in Fig. 7. In such cases, the ship motion might be suppressed due to the violent slamming or the green water caused by the wave #1. Accordingly, the slamming and the value of the maximum sagging moment the wave #2 might be suppressed. Further investigations on the cause of the suppression of the maximum sagging moment should be conducted.

The maximum sagging moments measured in all the cases (BF7, BF9, irr3, irr20 and BF9(FP)) are shown in Fig. 11. In all cases, the linear trend between the maximum sagging moment and the encounter wave height are observed. There are also much lower sagging moments than this linear trend.

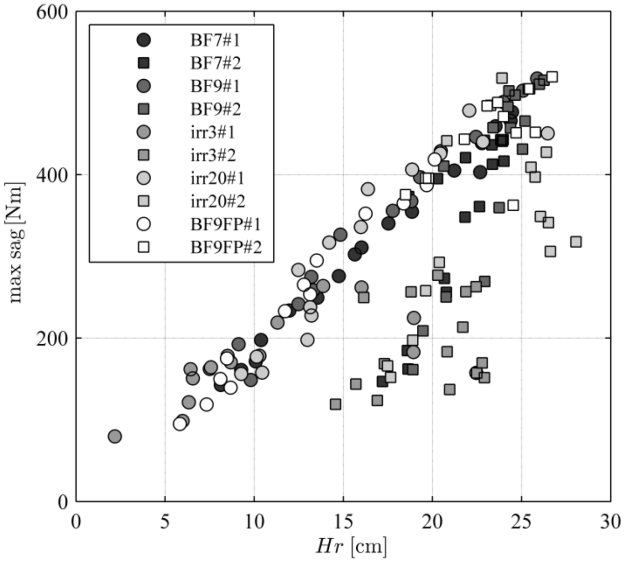

Fig. 11 Maximum sagging moments at S.S.5 plotted against encounter wave height. All the experimental cases are included.

4 Conclusion

Unidirectional modulational wave trains and freak waves in unidirectional irregular waves were produced in ASMB, and towing experiments with an elastic container ship were conducted in these wave fields. The geometry of these waves varies from leaning forward to leaning backward in the vicinity of the crest height maximum. Accordingly, the rear wave height reaches its maximum slightly after the crest height reaches its maximum. The experimental results reveal that the maximum sagging moments that occur on the model ship largely varies as a function of encounter timing. In most cases, the largest rear encounter wave heights were observed slightly after the crest height reaches its maximum. Accordingly, the largest maximum sagging moments occurred. The maximum sagging moments were linearly increased with the rear encounter wave height.

These experimental results (the variation of the wave geometry, the variation of the maximum sagging moments, the correlation between the encounter rear wave height and the maximum sagging moments) were common in all the cases with modulational wave trains and freak waves in irregular waves. Therefore, the vertical responses of the model ship reported here might be general for freak waves in wave groups.

Acknowledgment

We thank Dr. Sawamura for his support in the design of the elastic model ship. The calculation of the natural frequency of the elastic model ship with the NASTRAN was conducted by Dr. Oka, which is appreciated. We thank Dr. Kuroda and Mr. Kawamura for their assistance in conducting experiments. We also thank Dr. Tamashima and Ms. Sato for conducting the bending test of test pieces of the model ship and the manufacture of the elastic model ship.

This work was partially supported by JSPS KAKENHI (Grant Number 25249126).

Appendix Design of the elastic model ship

The design of the elastic model ship used in the experiment is summarized in this Appendix. The vertical bending stiffness should be scaled as follows to satisfy the elastic response:

$$(EI)_m = \alpha^5 (EI)_s. \quad (3)$$

Here, E, I and α denote the Young's modulus, the moment of inertia of area and the length scale between the full-scale ship and the model ship. Subscripts m and s denote the model ship and the full-scale ship.

The elastic model ship is composed of the unsegmented hull and the backbone (see Sawada *et al*. [21]). The hull is made of urethane foam, and aluminum channels are used as a backbone. The vertical bending stiffness of both the aluminum channel and the urethane hull is taken into account for the design of the elastic model ship. The hull of an unsegmented model ship is more continuous and smoother than that of a segmented model ship.

The aluminum channel is fixed to the aluminum bulkheads equipped at the interval of S.S.1 from S.S.1.5 to S.S.8.5. Strain gauges are attached to this aluminum channel at the interval of S.S.1 from S.S.2 to S.S.8. Vertical bending moments at each square station are evaluated from the strains measured on the aluminum channel.

The longitudinal distribution of the vertical bending stiffness and the height of the neutral axis were designed to be similar to the subject ship in the range from S.S.2.5 to S.S.7.5. A schematic view of the cross-section of S.S.5 is shown in Fig. 12(a). Two aluminum channels are bound together as in Fig. 12(b), and used as a backbone. The length b_u and b_l longitudinally vary by cutting the aluminum channels so that the similarity of the longitudinal distribution of the vertical bending stiffness and the height of the neutral axis is satisfied (see Fig. 13). The designed longitudinal distributions of the vertical bending stiffness is shown together with the prototype in Fig. 2. The similarity was validated by the three-point bending test (see Fig. 2). The longitudinal distribution of the height of the neutral axis of the prototype is linearly approximated from S.S.2.5 to S.S.7.5 (see Fig. 14). The height of the neutral axis of the model is adjusted to this linear approximation. The natural frequency of the model was validated by the hammering test (see Table 2). The similarity of the elastic characteristics was then ascertained.

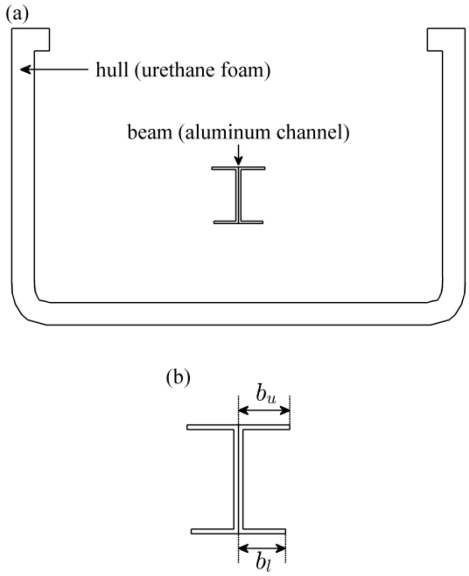

Fig. 12 (a) Schematic view of the cross section (S.S.5) of the elastic model ship. (b) Enlarged view of the aluminum channel.

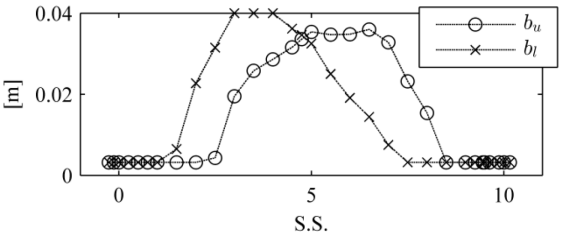

Fig. 13 Longitudinal distribution of the length b_u and b_l of the aluminum channel.

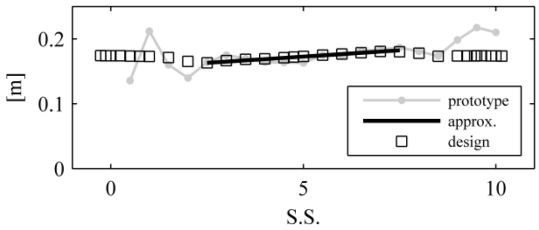

Fig. 14 Longitudinal distribution of the height of the neutral axis.

References

[1] Janssen, P. A. (2003) "Nonlinear four-wave interactions and freak waves", *Journal of Physical Oceanography*, *33*(4), pp.863-884

[2] Mori, N., & Janssen, P. A. (2006) "On kurtosis and occurrence probability of freak waves", *Journal of Physical Oceanography*, *36*(7), pp.1471-1483

[3] Waseda, T. *et al.* (2009) "Evolution of a random directional wave and freak wave occurrence", *Journal of Physical Oceanography*, *39*(3), pp.621-639

[4] Benjamin, T. B., & Feir, J. E. (1967), "The disintegration of wave trains on deep water Part 1. Theory", *Journal of Fluid Mechanics*, *27*(03), pp.417-430.

[5] Yamamoto, Y. *et al.* (1984), "Disastrous damage of a bulk carrier due to slamming", *Naval Architecture and Ocean Engineering*, *22*, pp.159-169

[6] Clauss, G. F. *et al.* (2011), "Influence of wave group characteristics on loads in severe seas", In *ASME 2011 30th International Conference on Ocean, Offshore and*

Arctic Engineering, pp.685-692. American Society of Mechanical Engineers.

[7] Fedele, F. (2014), "Geometric phases of water waves", *EPL (Europhysics Letters)*, *107*(6), pp.69001

[8] Kurimoto, M. (2006), "Generation and visualization of extreme waves based on dispersive focusing and directional focusing mechanism", Bachelor's thesis, the University of Tokyo (in Japanese)

[9] Banner, M. L. *et al.* (2014), "Linking reduced breaking crest speeds to unsteady nonlinear water wave group behavior", *Physical review letters*, *112*(11), pp.114502

[10] Houtani, H. *et al.* (submitted), "Experimental and numerical investigations on temporally periodic and spatially periodic modulational wave trains", *Journal of Fluid Mechanics*

[11] Tanizawa, K. *et al.* (2010), "The actual sea model basin" , *Papers of National Maritime Research Institute*, *10*(4), pp.1-40 (in Japanese)

[12] Yamamoto, Y. *et al.* (1980), "Motion and Longitudinal Strength of a Ship in Head Sea and the Effects of Non-Linearities", *Naval Architecture and Ocean Engineering*, *18*, pp.91-100

[13] Waseda, T. *et al.* (2013), "On the generation of spatially periodic breather in a wave tank", In *ASME 2013 32nd International Conference on Ocean, Offshore and Arctic Engineering,* pp.V005T06A065. American Society of Mechanical Engineers.

[14] Houtani, H. *et al.* (2015), "Freak wave generation in a wave basin with HOSM-WG method", In-*ASME 2015 34th International Conference on Ocean, Offshore and Arctic Engineering,* pp.V007T06A085. American Society of Mechanical Engineers.

[15] West, B. J. *et al.* (1987), "A new numerical method for surface hydrodynamics" *Journal of Geophysical Research: Oceans (1978–2012)*, *92*(C11), pp.11803-11824

[16] Dommermuth, D. G., & Yue, D. K. (1987), "Numerical simulations of nonlinear axisymmetric flows with a free surface" *Journal of Fluid Mechanics*, *178*, pp.195-219

[17] Biesel, F. *et al.* (1951), "Les appareils générateurs de houle en laboratoire", *La Houille Blanche*, *6* (2) (4) (5)

[18] Kinoshita, T. *et al.* (2006), "Investigation of freak wave induced loads on a large container ship", In *26th Symposium on Naval Hydrodynamics, 3*, pp.211-218.

[19] Minami, M. *et al.* (2006), "Study of ship responses and wave loads in the freak wave", In *The Sixteenth International Offshore and Polar Engineering Conference*, pp.272-278. International Society of Offshore and Polar Engineers.

[20] Shi, J. *et al.* (2007), "Structural and motion responses on large container ships in freak waves", In *Reports of RIAM Symposium No.17SP1-2, Proceedings of a Symposium held at Research Institute for Applied Mechanics, Kyushu University*, *Kasuga, Fukuoka, Japan,* Article No.06

[21] Sawada, H. *et al.* (1987), "On an elastic model to simulate elastic hull responses of ships", *Papers of Ship Research Institute*, *24*(2), pp.153-166 (in Japanese)